Competitive internal transfers in metastable decay of cluster ions

E. Buonomo, F. A. Gianturco, G. DelgadoBarrio, S. MiretArtés, and P. Villarreal

Citation: J. Chem. Phys. **100**, 6472 (1994); doi: 10.1063/1.467056
View online: http://dx.doi.org/10.1063/1.467056
View Table of Contents: http://jcp.aip.org/resource/1/JCPSA6/v100/i9
Published by the American Institute of Physics.

Competitive internal transfers in metastable decay of cluster ions

E. Buonomo and F. A. Gianturco
Department of Chemistry, The University of Rome, Cittá Universitaria, 00185 Rome, Italy

G. Delgado-Barrio, S. Miret-Artés, and P. Villarreal
Instituto de Matematicas y Fisica Fundamental CSIC, Serrano 123, 28006 Madrid, Spain

(Received 22 November 1993; accepted 27 January 1994)

In a previous study of fragmentation patterns of $(Ar)_3^+$ clusters [G. Delgado-Barrio, S. Miret-Artés, P. Villarreal, and F. A. Gianturco, Z. Phys. D **27**, 354 (1993)] it was found that overall rotations control the lifetimes of the occupied metastable states of the cluster and that a spherical, effective interaction was sufficient to describe the dynamical process. In the present study, the strong anisotropy of a more realistic three-particle interaction is introduced and its effects on metastable decay are examined. By separating internal rotations from internal vibrations of the diatomic ion, it is possible to show that internal predissociation pathways are very efficient and lead to very short lifetimes. The latter can be lengthened only when overall rotational states are directly included, thus confirming the physical picture of the earlier work.

I. INTRODUCTION

The unimolecular decomposition mechanism which presides over the dissociation of metastable states in ionic clusters is currently a subject of very active research, both experimentally and theoretically.[1–3] Such processes are usually started by forming neutral aggregates in supersonic expansion beams and by further ionizing them with laser excitation after the nozzle expansion.[4] Detailed experimental results are, in fact, often difficult to obtain since the above supersonic expansions usually lead to a distribution of different cluster sizes. This means that the most elegant way to circumvent the problem is to ionize the clusters and then select them by mass spectrometry, thus yielding extensive data over the original neutral cluster distributions but also raising doubts over a unique relation existing between the measured cluster ion distributions and the original neutral cluster size distribution.[5]

In the case of rare-gas clusters, the possible structures of the smaller species are simple enough that one could attempt a detailed understanding of possible dynamical pathways from the knowledge of the interaction forces as obtained from accurate *ab initio* calculations.[6] In particular, the photodissociation of argon cluster ions by electron bombardment has provided a wide variety of data[7] on the possible electronic states involved and on the relative lifetimes of the observed photofragments. Moreover, Märk and co-workers[8] have demonstrated a while ago that small argon clusters comprised of as few as three atoms can display metastable decays in time regimes extending beyond 10 μs after the ionization event. Since it was also found that even the dimer ion[9] could display long-time metastability, it has been suggested that centrifugal effects could be responsible for such unusually long lifetimes[10,11] in the trimer clusters.

We have recently examined in detail[12] this aspect of the fragmentation dynamics of $(Ar_3)^+$ clusters and found out that accurate quantum calculations of predissociative lifetimes indeed span a very wide range of time intervals once the overall rotational temperature of the original cluster is increased to fairly large values of total angular momentum J. In other words, the physical picture which emerges from the previous studies describes the metastability of the cluster ions as mainly due to the overall rotational motion of the ionic complex, without any specific reference to either the rovibrational energy content of the diatomic fragment, Ar_2^+ or to the coupling of its internal degrees of freedom with the unimolecular dissociative coordinate mediated by the full anisotropic interaction of the three-particle system.[6,13]

In the present study we therefore wish to address the additional problem, with the view of further increasing the level of realism employed to treat the fragmentation dynamics, by considering the coupling between the existing internal motions within the ionic cluster and the overall rotational motion of that cluster. The possible, alternative pathways for the dynamical breakup of the metastable states are, in fact, very important for gaining an accurate overall picture of the microscopic processes which control the growth and destruction of ionic clusters formed after nozzle beam expansions. We are dealing here with a special situation, in comparison with the more traditional cases of neutral van-der-Waals (vdW) systems,[14,15] in which the molecular (diatomic) partner is a strongly bound ionic state, i.e., the $^2\Sigma_u^+$ state of Ar_2^+, and the third atom in the complex is also bound to it via a very deep and anisotropic potential energy surface (PES) that is likely to strongly couple the relative motion within the complex and the ionic diatom internal degrees of freedom. Whether or not such a coupling plays an important role in the metastability of the ionic complex is the subject of the present study.

Section II briefly describes the overall interaction forces in $(Ar_3)^+$ and then their analytic representation in the present computations, while Sec. III gives in more detail the theoretical treatments of the fragmentation dynamics which we have carried out. Section IV reports the results of our calculations and discusses them vis á vis the existing experimental findings. Our final conclusions are summarized in Sec. V.

II. THE ANISOTROPIC INTERACTION FORCES

As mentioned above, configuration interaction calculations were carried out for the system $Ar–Ar_2^+$,[6] using all

 0021-9606/94/100(9)/6472/15/$6.00

three coordinates, i.e., the two atom–atom distances and their relative orientation. The level of the all-electron approach (53 electrons) was used for all points and the correlation effects were introduced via the well-known multireference double configuration interaction (MRDCI) technique,[16] with a selection threshold of 2.5 μh which lead to a selected subspace of configurations of the order of 12 000.

The isolated diatomic ion, Ar_2^+, was analyzed first and several of its electronic states were computed over an interval of relative distances between 4.0 and 20.0 a_0.[6] The various features of the ground state ($^2\Sigma_u^+$) and of the first excited state ($^2\Pi_g$) were obtained by polynomial fitting, producing for the former potential curve a minimum position, R_{eq}, of 4.64 a_0, a well depth of 1.19 eV and a rotational constant, B_e, of 0.138 cm^{-1}. The harmonic frequency was also found to be of 291.0 cm^{-1}. If one uses the above quantities within a Morse functional representation of the potential curve, one finds that the ionic diatom supports 64 vibrational bound states with an α value of 0.88 a_0^{-1} and an inflection point of 5.41 a_0.

The corresponding MRDCI calculations for the three-particle system had been carried out for $\theta=0°$ (collinear), $\theta=45°$, and $\theta=90°$ (perpendicular), using the Jacobian coordinates of R, from the approaching Ar atom to the center of mass (c.m.) of Ar_2^+, of r, the Ar_2^+ internuclear distance, and of θ, their relative orientation. The values of the dissociative coordinate R had been varied between 20.0 and 4.5 a_0 for four values of r, i.e., for $r=4.14$, 4.64, 5.14, and 6.14 a_0. The corresponding CI secular equations varied between 13 000 near equilibrium and 6000 in the dissociation channel with $R \gg r$.

In the collinear approach, minima in the potential were found for each r distance of the Ar_2^+ target. The estimated full-CI calculations suggested a global minimum at $R=7.82$ a_0, $r=4.64$ a_0, and a well depth of 0.15 eV. The perpendicular approach on the other hand, showed a basically different behavior with only very shallow minima in the various potential curves as function of r: The Ar_2^+ is left essentially unchanged and an overall minimum was found for $r=4.64$ a_0 and $R=6.9$ a_0, with a well depth of only 0.0025 eV.

The calculations therefore show that Ar_3^+ can be considered an actual molecule, with its collinear symmetric conformation being the most stable structure. On the other hand, the T-shape arrangement shows that its Ar_2^+ component is essentially unchanged from the isolated, diatomic ion and places the third Ar atom at a distance which is very nearly the same as in the neutral Ar_2 vdW dimer. Thus, no *chemical bond* appears to be formed in the latter approach and the interaction of Ar with Ar_2^+ could be described by the electrostatic behavior of an ion with an induced dipole, whereby the long-range interaction is proportional to the neutral atom polarizability α: $V_T(R) \sim -\alpha/2R^4$. This clearly means that one expects that the interaction varies quite dramatically as the angular, internal coordinate is changed and therefore that the usual multipolar expansion of full PES, written as

$$V(R,r,\theta)=\sum_{\lambda=0}^{\lambda_{max}} V_\lambda(R,r)P_\lambda(\cos\theta) \tag{1}$$

TABLE I. Morse-potential parameters obtained from least-square fittings of the MRDCI points of Ref. 17 at the three available orientations. See Eq. (2) for the meaning of symbols.

θ	R_m/Å	α/a_0^{-1}	D_e/eV
0°	4.13	0.797	0.08
45°	4.34	0.785	0.015
90°	3.65	0.773	0.03

should include rather large values for the multipolar index of the coefficients of the expansion (1) in order to reach an acceptable level of convergence in it.

A first step in the analytic representation of the full PES above could be attained by generating the rigid-rotor (RR) potential associated with Eq. (1) for the internuclear distance of $r=4.64$ a_0, i.e., one can first write, for each of the available angular orientations, that the corresponding curve is given by a Morse-type least-square fit of the existing points

$$V(R,r_{eq};\theta_1)=D_e(\theta_1)(\exp\{\alpha(\theta_1)[R_m(\theta_1)-R]\}-1)^2 - D_e(\theta_1). \tag{2}$$

The corresponding values of the Morse parameters obtained from the calculations of Refs. 6 and 17 are listed in Table I, while a general plot of the energy levels is shown in Fig. 1. One sees clearly from Fig. 1 that the overall potential presents two different regions of minima with a barrier between them as the orientation moves from $\theta=0$ to $\theta=\pi/2$. The corresponding anisotropy is therefore rather strong, as gleaned from the behavior of the coefficients in Eq. (1) that were obtained by numerical quadratures at each relative distance value, R,

$$V_\lambda(R,r_{eq})=\frac{2\lambda+1}{2}\int_{-1}^{1} V(R,r_{eq},\theta)P_\lambda(\cos\theta)d\cos\theta. \tag{3}$$

The even values of λ involved were 0, 2, and 4. Their general shapes are shown in Fig. 2. It is interesting to note that the strong orientational anisotropy of the interaction is clearly exhibited by the relative strengths of the expansion coefficients around their well regions: The V_4 coefficient, in fact, shows the largest well depth to try to represent the double well feature of the surface of Fig. 1. On the other hand, the spherical term only exhibits a rather shallow well which monotonically increases as λ increases. The special feature given by this short-range anisotropy will be reflected in the dynamical behavior of the metastable states, as we will discuss below, once one considers the situations in which sizeable internal energy is stored in the dimer rotational motion and can cause predissociating breakup of the cluster ions.

The next step in constructing the full interaction is to allow for the diatomic vibrational motion and for its changes as the argon atom approaches the ionic fragment from different directions. The MRDCI calculations[6] have already shown that the T-shape orientation produces very little deformation of the diatomic oscillator, as it keeps essentially the same bound distance of its asymptotic value during the argon ap-

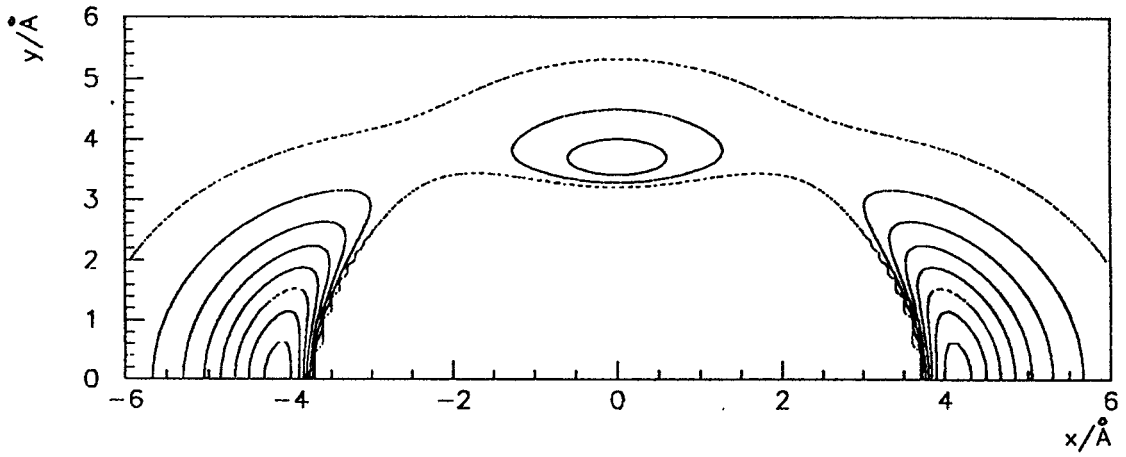

FIG. 1. Computed potential energy surface for $Ar-Ar_2^+$ from a Morse-type fitting of MRDCI points. The Ar_2^+ is kept at its equilibrium distance of 4.64 a_0. The distance from the c.o.m. are given in Å.

proach down to rather short R values. Thus, we may expect that rather little coupling occurs between the dissociative coordinate of the trimer ion and the vibrational energy content of the ionic dimer during the breakup of possible metastable states.

The collinear surface, on the other hand, exhibits much more marked structural details.[6,13] A decrease of the R coordinate definitely leads to a marked increase in the r values and to a charge redistribution over all three nuclei, so that one might describe this approach more like the formation of a chemical bond with the lowest energy structure possessing almost equal bond lengths. Consequently, we would expect that such geometries of the cluster complex lead to rather strong couplings between metastable fragmentation and vibrational energy content of the dimer ion. The argon approach under 45° finally shows[6] repulsive behavior as in the T-shape conformation for small separations in Ar_2^+ (r=4.14 and 4.64 a_0) but also exhibits minima, as in the collinear approach, for values of r=5.14 a_0. In other words, the *bent* approach shows a general behavior which is intermediate

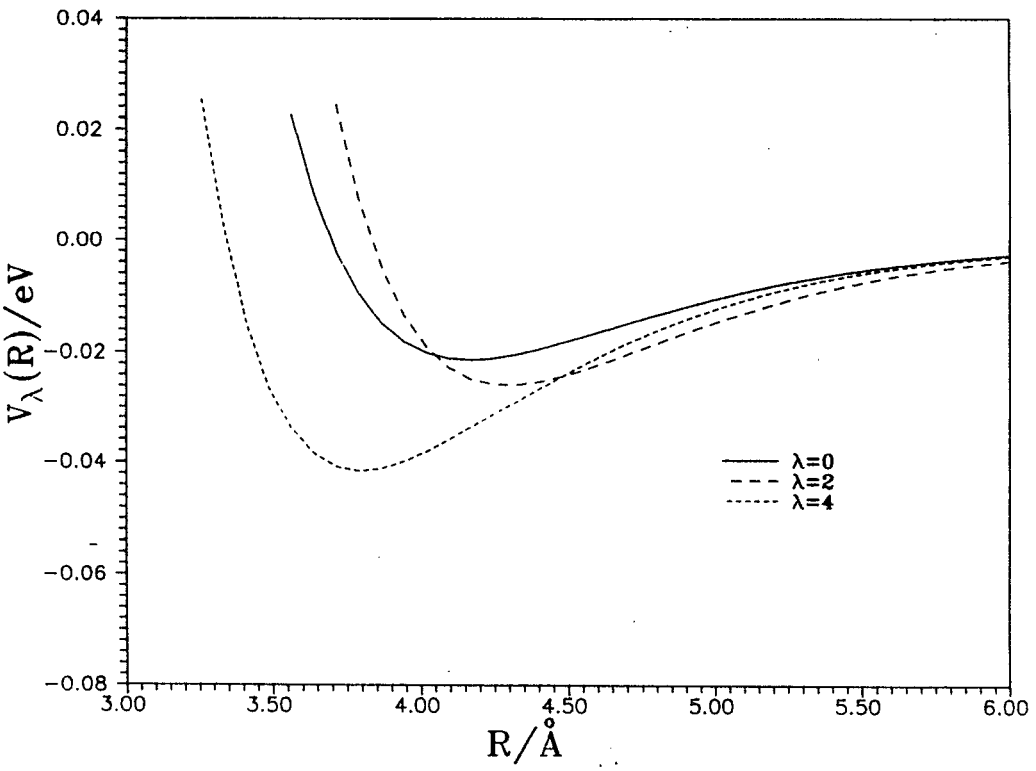

FIG. 2. Multipolar expansion coefficients (even λ values) of the rigid-rotor potential function for $Ar-Ar_2^+$. Distances are in Å and energy values in eV.

between the two previous orientations, with the appearance of some sort of chemical bonding at a shorter distance and with a somewhat *stretched* dimer ion state.

In order to realistically model the various features of the PES discussed above, we have tried to put together a least-square fitting of the existing computed points[13] in the form of a Morse-type potential function with parameters that depend on the orientation and the collision coordinates of the cluster ion:

$$V(R,r,\theta)=D_e(R,\theta)(\exp\{\alpha(R,\theta)[\bar{r}(R,\theta)-r]\}-1)^2 - D_e(R,\theta). \quad (4)$$

The possible θ values were those available from the MRDCI calculations mentioned before,[6] i.e., $\theta=0°$ and 90°. Each Morse function was produced to fit the four available r values between 4.14 and 6.14 a_0 for nine different values of R at each orientation. In order to properly scale the asymptotic reference of each *vibrational* potential, the D_e value of the isolated Ar_2^+ was approached for the largest R value available ($\sim 9\ a_0$). As a consequence of the large orientational anisotropy mentioned before, the corresponding parameters of the Morse function describing the target change quite dramatically as the R values decrease down to the trimer equilibrium geometry. In fact, because of the nature of the Jacobi coordinates in the collinear arrangement, we know that large r values and small R values lead to very repulsive potential shapes and a sort of *mirrored Morse* behavior of the diatomic ion potential in the presence of the third argon atom. Thus, the potential parameters in Eq. (4) depend very strongly on the chosen R value and indicate that the correct coupling between the dissociative motion and the internal vibrational motion of the ionic dimer during possible predissociative breakups can only be described if a much larger grid of Jacobi coordinate values were available from the MRDCI calculations. Since this is not presently the case, we concluded that our attempted fit on the vibrational dependence could not yet be reliably used in dynamics calculations but should wait insted for a more extensive recalculation of the whole rotovibrational PES.

III. THE THEORETICAL MODELS

As mentioned in Sec. I, the specific scope of the present study is to analyze the effectiveness of alternative decay channels in the dynamical breakup of metastable states of ionic clusters, after having shown earlier on Ref. 12 that argon ionic trimers exhibit very long lifetimes only when they are produced at high rotational temperatures of the overall system. In particular, we wish to examine how effectively the internal degrees of freedom in the cluster, i.e., relative dimer ion rotations and dimer vibrations, can provide the coupling mechanisms that favor the cluster fragmentation and bypass the longer lifetimes existing for high levels of overall rotation of the complex.

We have seen in Sec. II that the full interaction of the ionic trimer exhibits a markedly anisotropic orientational dependence and that the corresponding vibrational motion of the dimer ion is coupled to the motion of the incoming Ar atom only along some of the possible orientations of approach. We could therefore start with a detailed analysis of the first of the possible competitive processes, i.e., the predissociative breakup of metastable clusters due to the internal coupling of dimer rotational motion with the bound *stretching* motion of the third argon atom. This will obviously be a case of rotational predissociation (RP) dynamics and is likely to be an important pathway because of the established strong anisotropy of the trimeric ion PES.

A. Rotationally predissociative breakup

Since the present system exhibits a rather strong chemical bonding region and closely spaced rotational levels of the ionic dimer, it requires highly excited rotational states of Ar_2^+ to be present in the cluster in order to cause an alternative pathway to other forms of fragmentation of possible metastable states. At the same time, the strongly anisotropic potential causes the vdW interaction to change markedly with orientation and to *lock* the target rotor into preferential geometries as those shown by the overall PES of Fig. 1. In other words, we are dealing here with a strongly hindered rotor which slowly precedes within the limited angular regions of either of the equilibrium basis n (for $\theta=0°$ and 90°) in which it happened to have formed the vdW ionic trimer. This implies that we could treat the pure coupling between diatomic rotational energy content and the dissociative motion of the faster argon atom in a simplified fashion through the so-called adiabatic angular (AA) approximation[18–21] which we often employed for neutral vdW systems. The model is closely related to the rotational IOS approximation used in scattering problems[22,23] and takes advantage of the presence of fast *vibrational* motion along R and of slow rotational motion of Ar_2^+, once we completely disregard the presence of either rovibrational coupling with vibrating ionic dimer or of high rotational states of the overall trimer complex, to partly decouple this type of relative motion when solving the bound-to-continuum processes within the RP fragmentations.

After separation of the center of mass of the whole system, the Hamiltonian for the relative nuclear motion may be written as

$$H=-\frac{\hbar^2}{2\mu}\frac{\partial^2}{\partial R^2}+\frac{\hbar^2\hat{l}^2}{2\mu R^2}+B_e\hat{j}^2+V(R,\theta) \quad (5)$$

most of the terms have been explained before and, $\hat{l},\hat{j}$ are the angular momentum operators associated with the $\hat{R}$ and $\hat{r}$, respectively. Whenever the *stretching* frequency along R is large compared with the Ar_2^+ rotational constant and the overall rotation constant associated with a reasonable mean value of $R(B_R=\hbar^2/2\mu\bar{R}^2)$, then we may write the discrete functions of the complex as products of a radial part ϕ_n and an angular function F

$$\Psi^D_{nm}(\mathbf{R},\hat{r})=\phi_n(R,\theta)F_{nm}(\hat{R},\hat{r}). \quad (6)$$

The indices (nm) describe now the quantum numbers for the R motion and the *bending* or precession in θ within the cluster. The average frequency along R is of the order of 40 cm^{-1}, while the Ar_2^+ rotational constant is ~ 0.15 cm^{-1}, and the B_R rotational constant, assuming $\bar{R}\simeq 7.7\ a_0$, is ~ 0.04

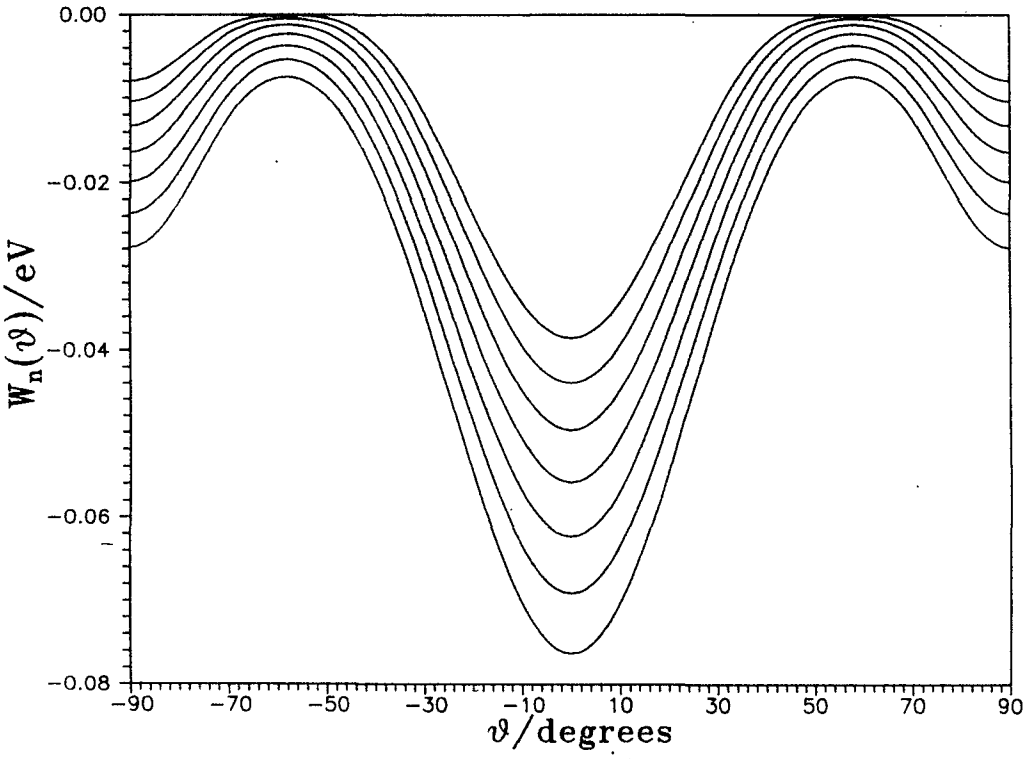

FIG. 3. Computed angular adiabatic potential energy functions, for n values from 0 to 6, for the Ar_3^+ cluster treated as a rigid rotor.

cm^{-1}. Thus, it becomes reasonable to assume the separation of Eq. (6) and to obtain the ϕ_n by solving the following equation of motion:

$$\left(-\frac{\hbar^2}{2\mu}\frac{\partial^2}{\partial R^2}+V(R,\theta)\right)\phi_n(R;\theta)=W_n(\theta)\phi_n(R;\theta), \quad (7)$$

whereby the radial functions have been treated as being *transparent* to the action of the angular momentum operators:

$$\hat{l}^2\Psi^D_{nm}=\phi_n\hat{l}^2F_{nm}, \quad (8a)$$

$$\hat{j}^2\Psi^D_{nm}=\phi_n\hat{j}^2F_{nm}. \quad (8b)$$

That the corresponding angular adiabatic potentials exhibit strong angular dependence can be seen from the plots reported in Fig. 3. We show there the seven bound state potentials supported by the ionic cluster and their behaviors as a function of θ : the barrier which exists around 60°, in going from the collinear to the T-shape minimum, confirms the findings of the potential energy surface of Fig. 1. Moreover, one clearly sees that the bending states defined by the index m will be strongly overlapping as n increases and therefore the expansion of Eq. (6) will need further refinements as we shall discuss below.

It is also interesting to see how much the corresponding bound functions for the *radial* motion along each angular cut of the original PES change as the relative orientation sweeps across the angular geometry. This is shown by the calculations reported in Fig. 4, where the plots in the upper part of the figure describe the bound $\phi_n(R;\theta)$ functions for $n=0$ and for three different angles: as the potential becomes more shallow the actual level moves up and nearer to the top of the corresponding well. This point is even more evident from the calculations represented in the lower part of the Fig. 4, where the bound functions for $n=4$ are reported. As the orientation moves to $\theta=45°$, in fact, the level goes up and correspondingly moves very near to the top of the well, which is now at its shallowest.

It is worth remembering, at this point, that the angular eigenvalues of Eq. (7) and of the plots in Fig. 3 now become effective potentials for the bending motion within the complex and allow us to obtain the *bending* angular functions of Eq. (6).[18] The latter are usually expanded via a body-fixed (BF) rotational basis set[24,25]

$$F_{nm}(\hat{R},\hat{r})=\sum_{j\bar{\Omega}} C^{(nm)}_{j\bar{\Omega}}\langle\hat{R},\hat{r}|JMj\bar{\Omega}\eta\rangle, \quad (9a)$$

where the parity index η is given by ±1 and

$$|JMj\bar{\Omega}\eta\rangle=[\mathscr{L}^{JM}_{j\bar{\Omega}}(\hat{r},\hat{R}) + \eta(-1)^J\mathscr{L}^{JM}_{j-\bar{\Omega}}(\hat{r},\hat{R})]\frac{1}{[2(1+\delta_{\bar{\Omega}0})]^{1/2}}. \quad (9b)$$

Moreover

$$\mathscr{L}^{JM}_{j\bar{\Omega}}(\hat{r},\hat{R})=\left(\frac{2J+1}{4\pi}\right)^{1/2}D^{J*}_{M\Omega}(\phi_R,\theta_R,0)Y^{\Omega}_j(\theta,\varphi). \quad (10a)$$

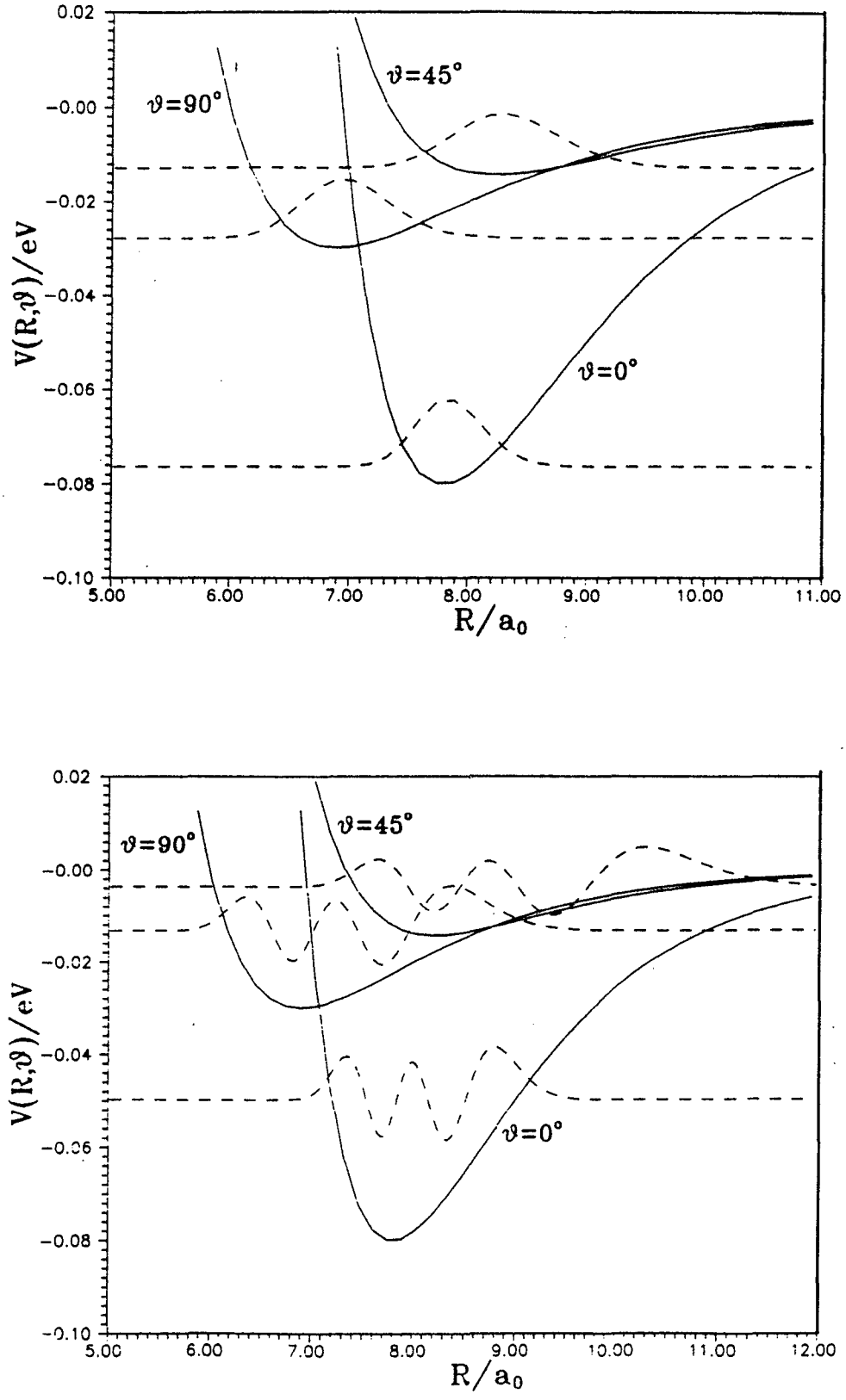

FIG. 4. Computed angular adiabatic functions [see Eq. (7)] for different value of the *stretching* quantum number n. Top part: for $n=0$ and different θ values. Bottom part: for $n=4$ and different orientations.

As a consequence of classifying the "bending" states by their symmetry index η also, then the effect of the $\hat{\ell}^2$ operator becomes the following for the off-diagonal matrix elements

$$\langle JMj\bar{\Omega}\eta|\hat{\ell}^2|JMj\bar{\Omega}+1\,\eta\rangle = -(1+\delta_{\bar{\Omega},0})^{1/2}*[j(j+1) - \bar{\Omega}(\bar{\Omega}+1)]^{1/2}[J(J+1) - \bar{\Omega}(\bar{\Omega}+1)]^{1/2} \quad (10b)$$

while it remains unaltered for the other matrix elements, as already discussed before.[18] We also keep the usual meaning of the various angular momenta[18] and (θ_R, ϕ_R) define the polar angles of $\mathbf{R}$ in a space-fixed (SF) frame of reference. Because of the strong anisotropy of the $W_n(\theta)$ potentials, and because of the depth of the interaction wells within the cluster, a large number of *bending* states is supported as bound by the present system, at variance with the usual situation of rather few F_{nm} bound functions which exist for neutral vdW complexes.[21] We shall see that such a situation plays a significant role in the dynamical development of our present model.

In order now to obtain the positive energy, continuum AA functions that describe the final, fragmented state of an Ar atom and of the diatomic ion Ar_2^+, we can therefore use the IOS approximation mentioned before[22] and write

$$\Psi^C_{j\bar{\Omega},\epsilon\bar{l}} = \phi_{\epsilon,\bar{l}}(R;\theta)\langle\hat{R},\hat{r}|JMj\bar{\Omega}\eta\rangle. \quad (11)$$

Thus obtaining the radial functions as a solution of the following equation:

$$\left(-\frac{\hbar^2}{2\mu}\frac{d^2}{dR^2} + V(R,\Theta) + \hbar^2\frac{\bar{l}(\bar{l}+1)}{2\mu R^2}\right)\phi_{\epsilon\bar{l}}(R;\theta) = \epsilon\phi_{\epsilon\bar{l}}(R;\theta), \quad (12)$$

where $\bar{l}$ represents the arbitrary index associated to the centrifugally sudden (CS) part of the IOS approximation[25] and describes essentially the overall rotational state of the three-particle complex. In the present calculations we chose to treat the $\bar{\ell}=0$ $(J=0)$ case in order to assess the pure contributions coming from possible RP breakup processes.

The energy of the continuum states is thus given by

$$E(j) = \epsilon + B_e j(j+1) \quad (13)$$

and the corresponding half-width for the rotationally induced fragmentation of a given $|nm\rangle$ metastable level may be calculated within the framework of the golden rule approximation

$$\Gamma_{nm} = \pi\sum_{j\bar{\Omega}} |V^{\mathrm{DC}}_{nm\to j\bar{\Omega}}|^2, \quad (14)$$

where the discrete-continuum couplings are given by

$$V^{\mathrm{DC}}_{nm\to j\bar{\Omega}} = \langle\Psi^C_{j\bar{\Omega},\epsilon}(\mathbf{R}\hat{r})|H|\Psi^D_{nm}(\mathbf{R},\hat{r})\rangle \quad (15)$$

which are calculated on the energy shell

$$\epsilon = E_{nm} - B_e j(j+1) \quad (16)$$

with

$$H\Psi^D_{nm} = E_{nm}\Psi^D_{nm}. \quad (17)$$

The all-important elements of Eq. (15) are evaluated by expanding the discrete stretching functions in terms of Legendre Polynomials

$$\phi_n(R;\theta) = \sum_k a_k^{(n)}(R)P_k(\cos\theta) \quad (18a)$$

and the quadratures involving continuum radial functions with a similar expansion

$$\langle\phi_{\epsilon\bar{l}=0}(R;\theta)|a_k^{(n)}(R)\rangle = \sum_\lambda f_{k\lambda}^{(n)}(\epsilon)P_\lambda(\cos\theta) \quad (18b)$$

one can evaluate all the contributions of H to Eq. (15) in terms of the radial coefficients of Eq. (18a) and the energy-dependent coefficients of Eq. (18b).[18] Since the actual developments have been given before[20,21] we refer the interested readers to these references for further details.

An example of the behavior of the solutions of Eq. (12), for various angular orientations is shown in Fig. 5. The stretching quantum number n is equal to 4, while the bending state considered is the one with $m=13$. From Eq. (16), the final, asymptotic rotational state is with $j_f=1$. One clearly sees the effect of the potential anisotropy, which makes the state still appearing as bound in the collinear orientation. It is worth mentioning at this point that, because of the antisymmetric nature of the electronic wave function of Ar_2^+, the corresponding rotational wave functions must be given by antisymmetric functions, i.e., only odd values of j are allowed for the diatomic rotor states. The parity of the nuclear functions for Ar_2^+ is, in fact, also that of a symmetric function. For that particular geometry one needs to include a much higher number of *bending* states before the local continuum is effectively reached. As an example, Fig. 6 shows the behavior of such a function for $n=4$, $m=49$, and the final state (rotational) $j_f=1$, in the collinear geometry: one clearly sees the fast bending oscillations and the fragmentation behavior as the partners separate for larger R values.

The expansion of Eq. (18a) provides radial coefficients for the bound stretching motion and describes the angular dependence of such states. The overlap of such coefficients with the corresponding continuum functions gives us a qualitative indication about the range of orientations for which the bound–continuum coupling is most likely to be effective. Thus, if we represent the overlap values from Eq. (18b) as function of the angle θ, and for chosen values of k and of ϵ, we could verify further the coupling strength of the interaction with dimer rotational levels.

The results in Fig. 7 show exactly such a behavior, obtained by computing the left-hand side of Eq. (18b) for various a_k coefficients in Eq. (18a). The continuum state which is being considered is for $n=0$, $m=19$, and the final rotational state of the fragment is chosen to be $j_f=1$.

It is interesting to note that, even for the $k=0$ coefficient, the bound-continuum overlap structure shows a very marked angular dependence, and is largest in the region of the barrier between the two minima in the collinear and T-shape geometries. This is in keeping with the idea that those regions of

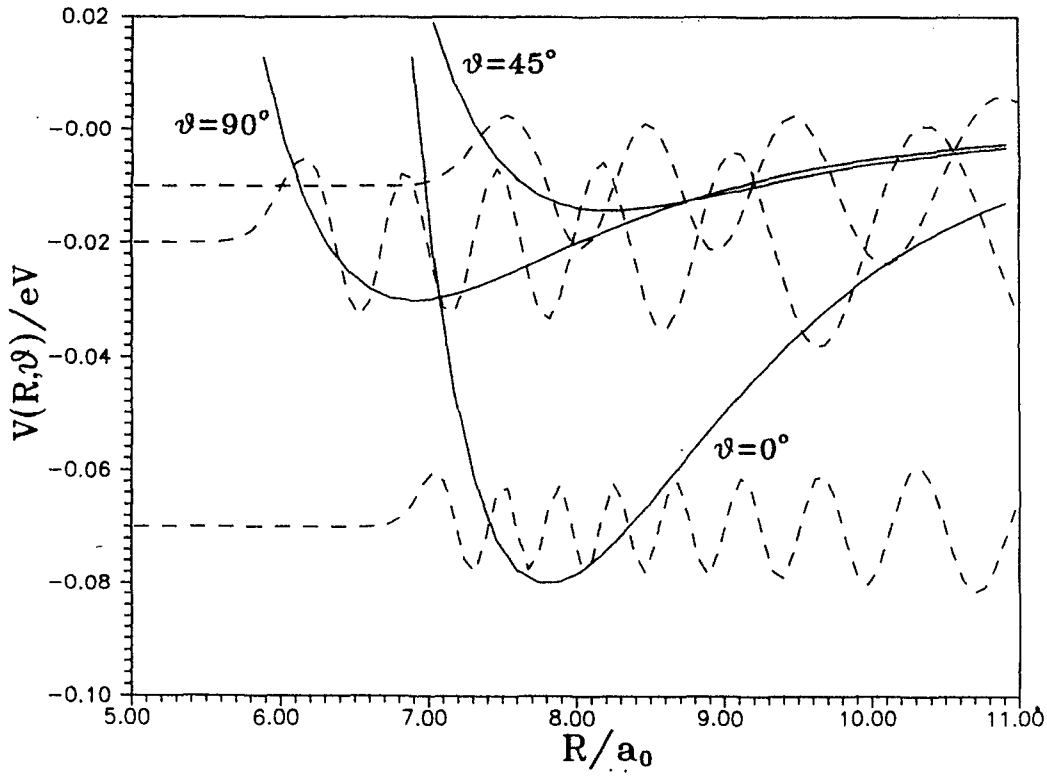

FIG. 5. Computed angular adiabatic dissociating functions of the ionic complex [Eq. (12)] for $n=4$, $m=13$, and $j=1$ in Eq. (16). The solutions at three different orientations are shown.

the effective potential $W_n(\theta)$ in which the potential well is the shallowest are also most efficient in inducing RP behavior in the system under study.

The results found above are also confirmed by the calculations of Fig. 8, where a different bound state is considered, i.e., the one with $n=4$ and $m=13$, and for which four different components with increasing polynomial indices of Eq. (18a) are examined. One clearly sees in the Fig. 8 that, as the k index becomes larger the oscillatory structure of the continuum increases and so does the angular region within which the overlap becomes significant. In fact, for $k=10$ one sees that the coupling extends now over a very broad range of angular values, while for $k=0$ only a rather narrow range of θ values around the potential barrier shows significant overlap with the bound function depicted in Fig. 5.

It is also interesting to note[18] that, if we now allow the system to rotate as a whole, i.e., if we choose in Eq. (12) values of the total angular momentum $J(=\bar{l})$ larger than zero, additional contributions appear in Eq. (15) and involve the overlapping of radial functions between the full *bending–stretching* bound states and the continuum states

$$\langle JMj\Omega|\langle\phi_{\epsilon\bar{l}}(R;\theta)|\phi_n(R;\theta)\rangle W_n(\theta)|F_{nm}(\hat{R},\hat{r})\rangle, \quad (19)$$

where one sees the effect of the angular adiabatic potential on the coupling between metastable states and dissociated fragments. An example of such potential coupling is shown in Fig. 9, for a particular continuum state with $\bar{l}=20$ and a bound state with $n=0$. The bending state of the complex is with $m=237$ and leads to $j_f=1$, as represented in Fig. 6 for $\theta=0$. One sees that once more the overlap (and hence the coupling) shows a maximum in the region of the barrier in the effective potential while all oscillations, as in Figs. 7 and 8, have produced a much more localized coupling region within each angular range. This feature of the present strong coupling requires very careful numerical stabilization in the expansion of Eqs. (18).

We are now in position of testing the relative probabilities of cluster breakup by rotational predissociation, i.e., of calculating the lifetimes of the metastable states produced in the cluster ion when enough internal rotational energy is stored in the ionic dimer during cluster formation.

IV. RESULTS FROM QUANTUM DYNAMICS

As mentioned before, the aim of the present study is to see, from realistic calculations, how competitive the RP channels could be in speeding up (or further slowing down) the lifetimes of the metastable cluster states observed experimentally.[8–11] This effect requires the knowledge of the diatomic energy content, i.e., the various asymptotic thresholds for the rotational levels populated after breakup, and furthermore the calculation of the bound states of the triatomic complex and of its metastable states. The actual RR potential energy surface will then provide the necessary coupling.

As an example of the existing density of states, we report in Table II the bound rotational levels of Ar_2^+, for energies of the order of the average energy available in the com-

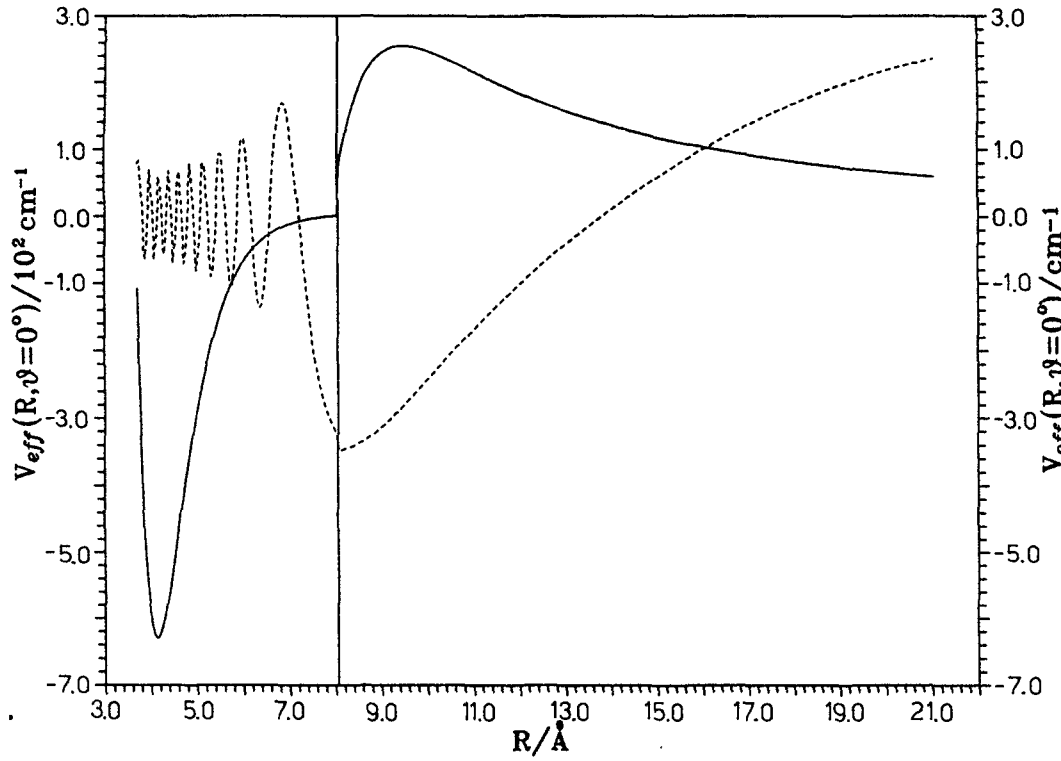

FIG. 6. Computed continuum function in the collinear orientation for $n=4$, $m=49$, and $j=1$ in Eq. (16). The solid line gives the shape of the potential which supports the state in question.

plex, i.e., the average well depth of the spherically averaged potential of Fig. 2. As one sees there, the small values of the B_e provides a very high density of rotational states and a near-continuum energy distribution in the fragmented rotor. This means that, during cluster formation, it would be reasonable to assume that a fair amount of energy can be stored in the rotor and further coupled to the other degrees of freedom of the complex which is being formed.

On the other hand, the complex itself presents a rather rich structure of bound and metastable AA states $|nm\rangle$. As discussed before, the vdW neutral complexes which we have previously studied[18–21] had a much sparser distribution of bound states and allowed possible couplings with the rotor states only with rather few of them. In the present case, on the other hand, Fig. 3 shows the numerous *stretching* states of the complex and an even more numerous set of *bending* states supported by each n level have been obtained from expansion (9).

As an example of the richness of the predissociating states which may exist, even at the zeroth order level of considering each $|nm\rangle$ state uncoupled with others, we report in Table III some of the E_{nm} levels with positive energy existing within the range of the bound rotor states of Table II. We also show in the table the calculated Γ_{nm} of Eq. (14), together with the final rotor state, $j(\max)$, which contributes the most to the $|j\Omega\rangle$ sum of Eq. (14). Its corresponding Γ is also shown in the last column of the table. All the calculations were carried out for $J=0$, i.e., without yet considering the competitive effects of the overall rotations of the complex.

It is interesting to note when examining the results of the table, that all RP processes are here rather efficient, i.e., lifetimes range between 10^{-9} and 10^{-12} s and never show the values of the order of microseconds which were detected experimentally. It is also clear from our calculations that a rather broad range of final rotor states is populated after RP breakup and therefore one could expect rotationally *hot* ionic dimers, as surmised in some experiments.[14,15]

As mentioned in our earlier work,[19] in systems where strong coupling is expected between m states belonging to different *stretching* quantum numbers in Eq. (7), one should really improve on expansion (6) by using a sort of configuration interaction (CI) approach

$$\Psi_k^D(\mathbf{R},\hat{r})=\sum_{n,m} a_{nm}^k \phi_n(R;\theta)F_{nm}(\theta) \tag{20}$$

hence, the usual Schrödinger equation

$$H(\mathbf{R},\hat{r})\Psi_k^D(\mathbf{R},\hat{r})=E_k\Psi_k^D(\mathbf{R},\hat{r}) \tag{21}$$

may be solved by representing the full Hamiltonian in the basis of expansion (20) and by further diagonalizing the corresponding matrix.[19] One can also approximate the operators which appear in each off-diagonal element, $H_{nm,n'm'}$, of the above matrix and treat them as first-order correction to the diagonal solutions associated to the isolated adiabatic states

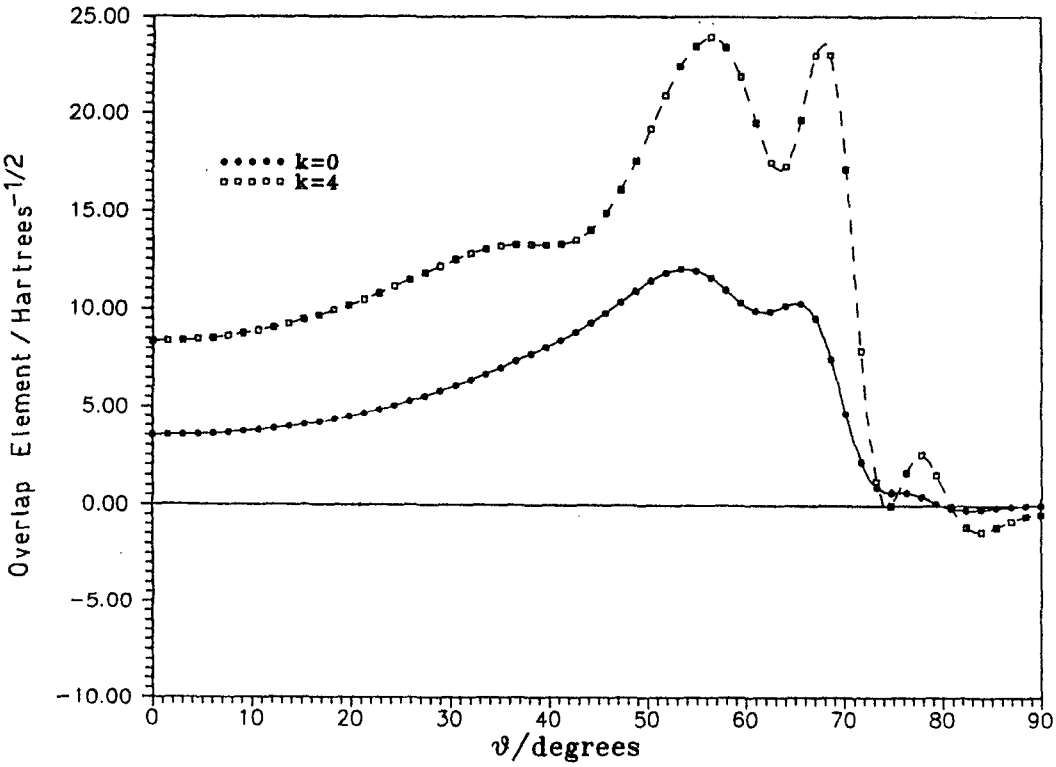

FIG. 7. Computed bound-continuum overlaps as a function of the angle of orientation within the cluster [Eq. (18b)]. The anisotropic coefficients of Eq. (18a) are fox $k=0$ and 4, while the *stretching–bending* complex state corresponds to $n=0$ and $m=19$. The final rotational state of Ar_2^+ is $j_f=1$.

of expansion (6).[19] When we looked at such corrections for the $n=0$ states of those listed in Table III, we found the following.

(i) The energy corrections varied between 1 and 2 cm^{-1} and generally pushed the levels more into the continuum.

(ii) The corresponding Γ values for the global process varied around 10%, thus the associated lifetimes remained of the same order of magnitude.

(iii) The individual $\Gamma_{j\Omega}$ changed more markedly (~20%) but the main final state remained the same and the associated lifetimes never changed order of magnitudes.

In other words, the first-order CI corrections modified the microstructure of the RP processes but did not change the previous physical picture of it being an efficient process for complex breakup.

The CI calculations employing about 560 states were also carried out for all of the levels obtained previously with the simpler, isolated adiabatic approach. The results for the lowest six states with positive energy are also shown in Table IV, together with their corresponding Γ values and lifetimes. It is interesting to note that the main effect of CI is to make the structure of the possible states richer than before and therefore to make the breakup process even more efficient: all the CI lifetime values, in fact, are now smaller than those computed in Table III and indicate that the nonrotating complex exhibits a more rapid breakup pathway if enough energy has been stored in the dimer rotor states.

In order to show the effect of having started with a complex with high rotational energy content in the dimer, we present in Table V the results of AA calculations, without CI effect, for highly energetic *stretching bending* $|nm\rangle$ states of the complex. It is interesting to see that, if one starts with an highly excited state of the complex, the RP probability is very strong to the neighboring levels but rapidly decays as we assume that the largest amount of energy released goes into the relative motion of the fragments. In other words, the calculations show that the RP process is very efficient even when the metastable state carries a high level of internal energy but that amount of energy is mostly left as dimer rotational energy.

The previous result for $J=0$, i.e., without allowing for the complex overall rotations but simply studying the competitive efficiency of RP fragmentations of metastable clusters, have shown us the following.

(i) When little energy is stored in the complex as internal energy, e.g., for $|nm\rangle$ states not far above the depth of the triatomic well, the corresponding fragmentation process is rather efficient with Γ values ranging from fractions of cm^{-1} up to 20–30 cm^{-1}. On the other hand, the range of orders of magnitude spanned is much narrover than that suggested by the experiments, i.e., it is only 3–4 orders of magnitude wide.

(ii) When the energy stored goes up to substantial fraction of the total well depth (which is ~1000 cm^{-1}), a process achieved with high bending quantum number values, the RP mechanism becomes even more effective but only a little energy is given up as relative energy. As a consequence, the calculations predict that the fragment diatomic ions are pro-

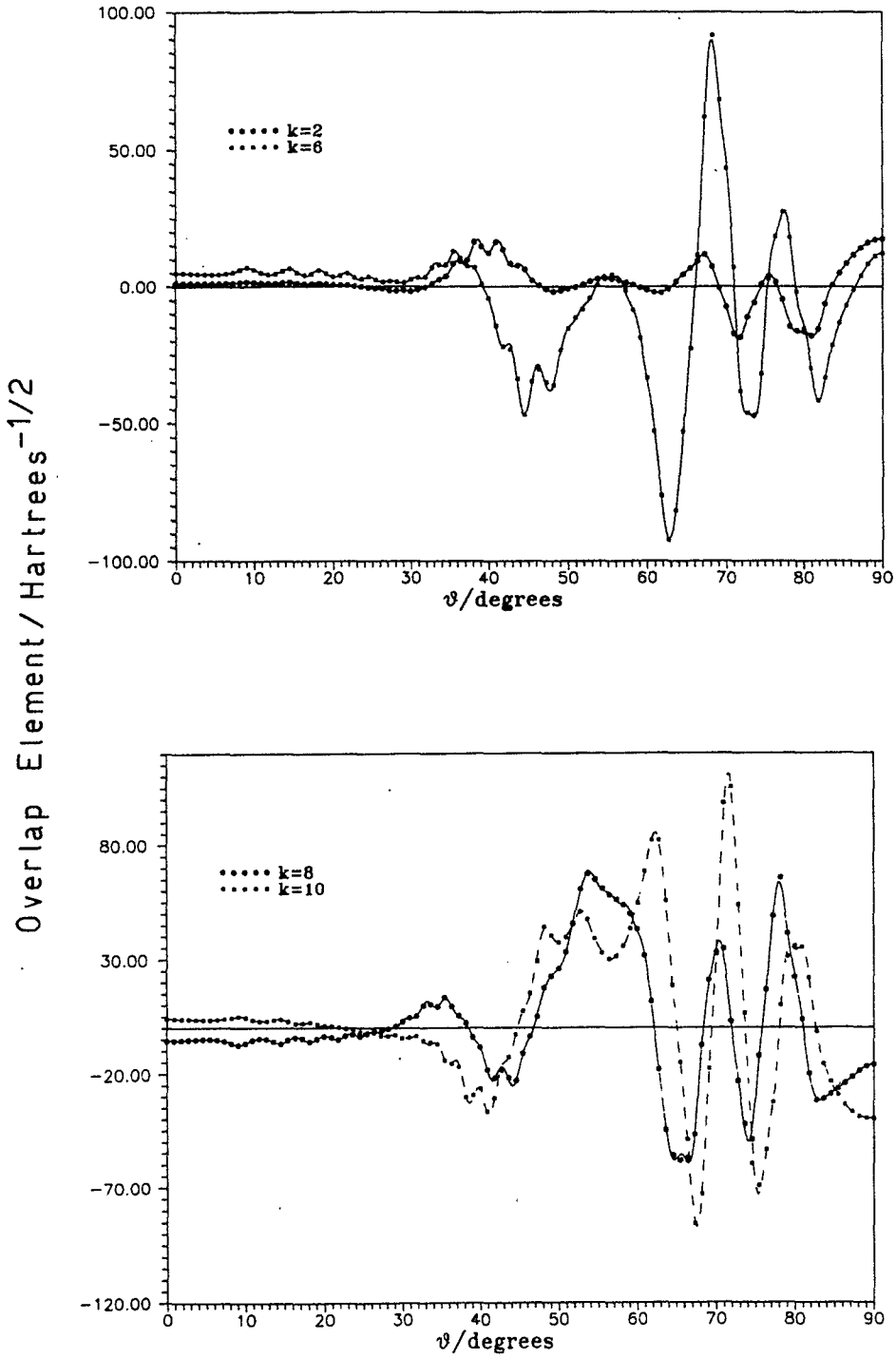

FIG. 8. Same as in Fig. 7, for different coefficients for bound states of the system. Top part: for $k=2$ and 6 and for the $|4,13\rangle$ bound state, with $j_f=1$. Bottom part: $k=8$ and 10 for the same bound state as before.

duced in highly excited rotational states. However, the corresponding lifetimes (see Table V for an example) never span more than two or three orders of magnitude, as was the case for less excited metastable states.

Let us now see, therefore, the effect of overall rotations on the computed relative lifetimes of the metastable cluster states. As examples of the many calculations which we carried out, we show in Table VI the range of lifetimes spanned by the lowest six metastable levels of the $n=0$ effective bending potential of Fig. 2 for different values of J, the centrifugal potential quantum number which describes the overall rotational states of the cluster ion.

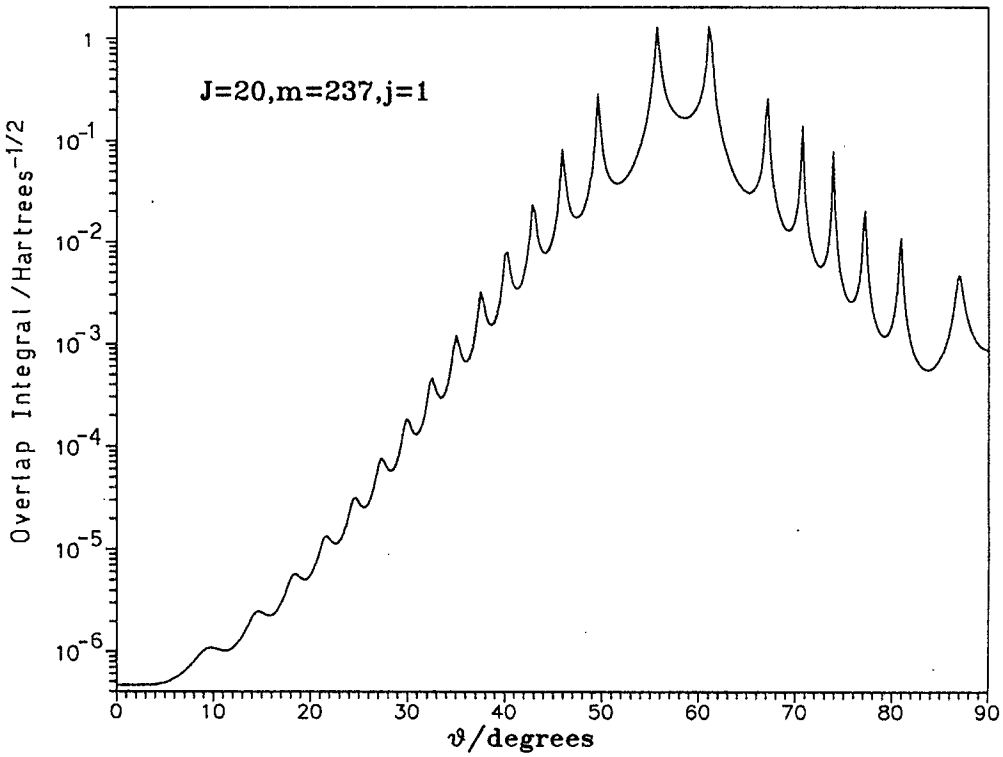

FIG. 9. Computed overlap integral for $n=0$ and $\tilde{l}=20$. The bending state of the complex corresponds to $m=237$ and the final rotational state of the fragment is $j_f=1$.

It is interesting to note the following.

(i) As J increases the possible states of Ω into which the complex can breakup increase and the linear coefficient of expansion (9) greatly vary across the examined range of lowly excited complex states.

TABLE II. Computed bound rotational levels for isolated Ar_2^+. The energies are given in units of eV and of cm^{-1}. The numbers in brackets are the exponents of 10.

j	E_j/eV	E_j/cm^{-1}
1	3.46(−5)	0.28
3	2.08(−4)	1.67
5	5.19(−4)	4.18
7	9.68(−4)	7.81
9	1.56(−3)	12.55
11	2.28(−3)	18.41
13	3.15(−3)	25.38
15	4.15(−3)	33.47
17	5.29(−3)	42.68
19	6.57(−3)	53.00
21	7.99(−3)	64.43
23	9.54(−3)	76.98
25	1.12(−2)	90.65
27	1.31(−2)	105.43
29	1.50(−2)	121.33
31	1.72(−2)	138.35
33	1.94(−2)	156.48
35	2.18(−2)	175.72
37	2.43(−2)	196.09
39	2.70(−2)	217.56
41	2.98(−2)	240.16

(ii) Because of the selection rules induced by the $\hat{l}^2$ and $\hat{j}^2$ operators, some of the initial bound states do not have neighboring states that are coupled to them and therefore their lifetimes dramatically increase.

(iii) As J increases the lifetimes of the metastable states considered cover a much wider range of values and become increasingly closer to those found experimentally[10,11] and produced by us earlier using theory.[12]

This is a very interesting result: since the system under consideration can be treated as a strongly hindered rotor, the triatomic cluster essentially achieves high internal energy values by reaching large values of the *bending* quantum number. This means, pictorially, that the third argon atom moves, in each of the regions with a well (either linear or T shaped) only within a rather narrow cone and strongly mixes the possible $|nm\rangle$ states with each other. The ensuing spreading of the coefficients of Eq. (9) controls the overall distribution into final, asymptotic rotor states, thus allowing for a much broader range of possible lifetimes as the overall rotational energy content increases. A pictorial representation of this result is shown in Fig. 10, where all computed lifetimes of Table VI are shown for the different overall rotational quantum number.

Another test that we felt needed to be carried out was to consider once more triatomic ions states with very large energy content above the allowed well depth of the complex. Thus, we carried out calculation with very large m values in the $n=0$ states and with positive energy of the order of 100 cm^{-1}. As the J values were increased, the number of pos-

TABLE III. Computed adiabatic angular bending–stretching states of the ionic clusters with positive energies. Total $J=0$. Quantum numbers and energies are given in the first two columns. The Γ of column three refers to all final states of the diatomic ion, while the Γ in the last column refers to the most probable final state j. The numbers in brackets are the exponents of 10.

n	m	$E(n,m)/\text{cm}^{-1}$	Γ/cm^{-1}	π/s	j (max)	$\Gamma(j)$
0	18	0.78	0.76(−3)	0.70(−8)	1	0.76(−3)
0	19	23.40	0.56(−2)	0.94(−9)	9	0.32(−2)
0	20	47.90	0.19(−1)	0.28(−9)	17	0.17(−1)
0	21	74.19	0.11(−1)	0.46(−9)	21	0.72(−2)
0	22	102.17	0.42(−2)	0.13(−8)	23	0.27(−2)
1	17	7.50	0.75(−1)	0.71(−10)	5	0.44(−1)
1	18	28.51	0.22	0.24(−10)	13	0.18
1	19	51.42	0.11	0.47(−10)	17	0.54(−1)
1	20	76.10	0.51(−1)	0.10(−9)	19	0.54(−1)
1	21	102.49	0.20	0.26(−10)	25	0.25(−1)
2	16	12.99	1.42	0.37(−11)	9	0.19
2	17	32.41	0.52	0.10(−10)	11	0.30
2	18	53.74	2.27	0.23(−11)	19	1.98
2	19	76.85	0.97	0.61(−11)	21	0.79
2	20	101.66	1.15	0.46(−11)	25	0.85
3	14	1.56	0.73	0.73(−11)	1	0.73
3	15	17.20	1.02	0.52(−11)	7	0.66
3	16	35.07	5.37	0.99(−12)	15	4.26
3	17	54.85	5.38	0.99(−12)	19	2.99
3	18	76.41	2.88	0.18(−11)	21	1.93
4	13	5.80	5.40	0.98(−12)	3	2.89
4	14	20.07	9.40	0.56(−12)	11	5.98
4	15	36.45	8.70	0.61(−12)	15	4.42
4	16	54.72	5.17	0.10(−11)	17	3.05
4	17	74.75	2.90	0.18(−11)	19	1.98
5	12	8.89	0.90	0.59(−11)	7	0.44
5	13	21.61	15.12	0.35(−12)	11	7.11
5	14	36.50	7.85	0.68(−12)	13	3.53
5	15	53.30	12.05	0.44(−12)	19	7.77
5	16	71.83	7.09	0.75(−12)	21	4.61
6	10	0.41	6.49	0.92(−12)	1	6.49
6	11	10.22	17.58	0.30(−12)	3	6.55
6	12	21.75	8.74	0.61(−12)	11	4.05
6	13	35.19	7.96	0.67(−12)	15	2.39
6	14	50.53	4.86	0.11(−11)	17	1.70

sible breakup, final channels reached values of 100–200 states. However, of such $|j\Omega\rangle$ states only less than 5% had linewidths of ~ 1 cm^{-1}, i.e., lifetimes in the picosecond range. The majority of them were associated to very long lifetimes due to the exclusion of couplings from the above selection rules. As a consequence of this result, the corresponding lifetimes could be either very short [when the coupling allowed included a state with a large coefficient in Eq. (9)] or very long when no particular coefficient dominated

TABLE IV. Computed lowest six E_k states of Eq. (21), and corresponding Γ values for each possible final state.

$\|k\rangle$	E_k/cm^{-1}	Γ_k/cm^{-1}	$j_{\max}$	$\Gamma_{j_{\max}}/\text{cm}^{-1}$	π/s[a]
93	0.50	2570	1	2.57	2.07(−12)
94	2.55	8.11	1	5.63	6.55(−13)
95	3.74	0.29	3	0.16	1.81(−11)
96	7.52	0.69	5	0.62	7.65(−12)
97	10.64	7.12	5	3.33	7.46(−13)

[a] $(-n)=10^{-n}$.

TABLE V. Computed angular adiabatic stretching–bending states with high rotational content. The individual RP widths are also listed. All values in cm^{-1}.

$\|nm\rangle = \|0,34\rangle$		$\|n,m\rangle = \|0,37\rangle$	
$E_{nm}=559.453$ cm^{-1}		$E_{nm}=707.106$ cm^{-1}	
$\Gamma_{nm}=4.56(-3)$ cm^{-1}		$\Gamma_{nm}=1.70(-4)$ cm^{-1}	
$\tau_{nm}=1.16(-8)$ s		$\tau_{nm}=3.12(-9)$ s	
j_f	$\Gamma_{j_f}/\text{cm}^{-1}$	j_f	$\Gamma_{j_f}/\text{cm}^{-1}$
61	3.57(−3)	69	1.24(−3)
⋮	⋮	⋮	⋮
51	1.94(−9)	59	1.66(−8)
⋮	⋮	⋮	⋮
41	3.29(−12)	49	6.23(−11)
⋮	⋮	⋮	⋮
21	1.269(−11)	29	1.26(−9)
⋮	⋮	⋮	⋮
11	3.95(−14)	19	1.52(−10)
⋮	⋮	⋮	⋮
1	4.71(−17)	1	2.74(−15)
⋮	⋮	⋮	⋮

TABLE VI. Computed energy levels and lifetimes of metastable states with different values of the rotational quantum number J. The states selected correspond to the lowest positive energy states for each J.

$\|nm\rangle$	E_{nm}/cm^{-1}	Γ_{nm}/cm^{-1}	τ_{nm}/s	$\|j\Omega\rangle$	$\Gamma_{j\Omega}/cm^{-1}$
$J=10$	0.94	0.30(−2)	0.18(−8)	|1,1⟩	0.28(−2)
|0,164⟩					
|0,165⟩	3.50	0.27(−2)	0.20(−8)	|3,2⟩	0.11(−2)
|0,166⟩	3.67	0.19(−2)	0.27(−8)	|3,0⟩	0.69(−3)
|0,167⟩	5.24	0.64(−3)	0.83(−8)	|5,2⟩	0.27(−3)
|0,168⟩	5.65	0.12(−1)	0.44(−9)	|5,1⟩	0.22(−2)
|0,169⟩	9.80	0.33(−2)	0.16(−8)	|5,4⟩	0.11(−2)
|0,170⟩	10.05	0.48(−2)	0.11(−8)	|7,5⟩	0.10(−2)
$J=20$					
|0,234⟩	1.44	0.32(−10)	0.17	|1,0⟩	0.28(−10)
|0,235⟩	1.98	0.44(−8)	0.12(−2)	|1,0⟩	0.27(−8)
|0,236⟩	2.29	0.32(−6)	0.17(−4)	|1,1⟩	0.24(−6)
|0,237⟩	3.45	0.22(−4)	0.24(−6)	|1,1⟩	0.11(−4)
|0,238⟩	5.28	0.34(−2)	0.15(−8)	|1,1⟩	0.12(−2)
|0,240⟩	6.90	0.18(−3)	0.30(−7)	|3,0⟩	0.79(−4)
|0,241⟩	7.21	0.11(−1)	0.50(−9)	|5,3⟩	0.39(−2)
$J=30$					
|0,232⟩	1.30	0.4(−30)	0.1(20)	|1,0⟩	0.3(−30)
|0,235⟩	3.38	0.3(−22)	0.2(12)	|1,1⟩	0.2(−22)
|0,236⟩	4.06	0.40(−10)	0.13	|1,0⟩	0.38(−10)
|0,238⟩	5.32	0.43(−8)	0.12(−2)	|1,0⟩	0.24(−8)
|0,239⟩	5.44	0.22(−8)	0.24(−2)	|1,1⟩	0.19(−8)
|0,244⟩	9.39	0.15(−1)	0.35(−9)	|1,0⟩	0.12(−1)
|0,245⟩	10.24	0.66(−1)	0.81(−10)	|3,0⟩	0.21(−1)

the expansion and therefore only inefficient transitions took part in the decay of the highly mixed initial state.

The conclusions of this last analysis are presented pictorially in Figs. 11 and 12, where the calculations of Table VI are reorganized in a different way. The results of Fig. 11 show the behavior of the RP lifetimes as function of Δm, which represents the difference between the index of the predissociating level and that of the last bound state in the relevant $|nm\rangle$ range. One clearly sees that, as J increases, the RP levels with largest lifetimes correspond to AA bound

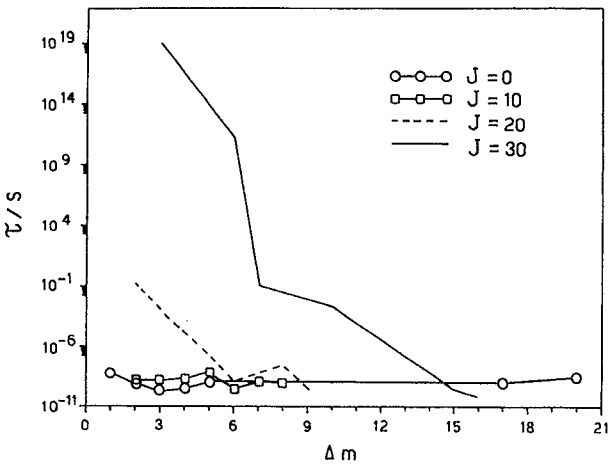

FIG. 11. Computed RP lifetimes as function of Δm, which represents the difference between the quantum number of the predissociating states and that of the highest bending bound AA states.

states very close to threshold, i.e., with small Δm. Accordingly, if one chooses an energy scale as in Fig. 12, one also sees that the least-efficient breakup processes correspond to the least strongly bound states of the trimer, and that no simple exponential energy dependence is shown by the computed RP times.

V. CONCLUSIONS

The calculations presented in this work further extend our previous analysis of the dynamical mechanisms which are likely to preside, at the microscopic level, over the fragmentation of metastable states existing in argon clusters ionized after their formation in a nozzle expansion. In particular, we have considered the internal structure of the PES in the trimer ion and have computed, from existing *ab initio* MRDCI calculations, model anisotropic potentials for the rigid rotor (RR) system and for the vibrotating complex.

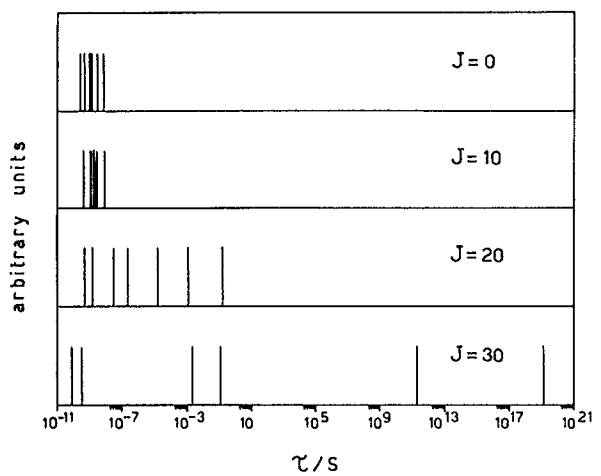

FIG. 10. Computed predissociating lifetimes of some trimers as function of the overall rotational quantum number J.

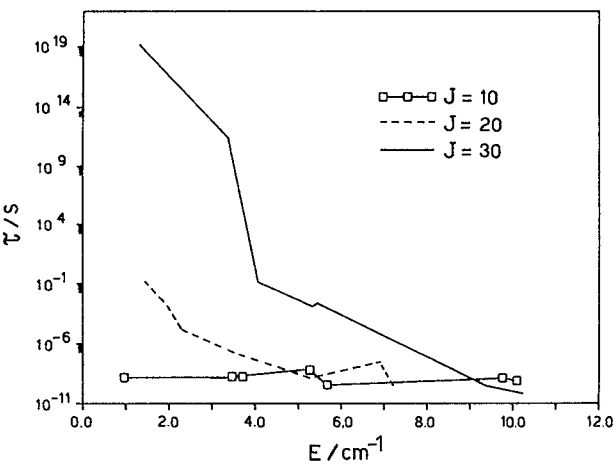

FIG. 12. Same as in Fig. 11 but as a function of the energy difference (in cm^{-1}) between the above states.

As a first step in increasing the complexity of the quantum dynamics calculations we have carried out rotational predissociation dynamics both in the case of a nonrotating complex and in various states of a highly rotating complex. The results of our calculations have clearly shown the following.

(i) Due to the special features of this ionic-bonded system, the anisotropic well depth supports several angular-dependent *stretching* states and an even larger number of IOS bending states. Moreover, due to the differences in time scales between the isolated rotating dimer and the internal *stretching* motion, one can reasonably expect that a partial decoupling between internal stretching and dimer rotations occurs during the breakup of metastable states;

(ii) When the dissociating dynamics are treated along the above lines, then one finds that RP processes are very efficient but span a narrow range of lifetimes, i.e., with τ values between 10^{-12} and $\sim 10^{-8}$ s. On the other hand, as the overall rotations are included, the ensuing complications in the selection rules acting on the couplings, and the increased number of possible final states which need to be considered, greatly increase the range of possible lifetimes which readily span values between 10^{-1} and 10^{-11} s. These values agree with those suggested by the experiments[10,11] and produced by our earlier calculation without internal structures in the complex.[12]

These results therefore indicate that, even when the internal rotations are taken into account, the dominating physical reason for observing a broad range of lifetimes is the possible existence of rotationally *hot* ionic complexes rather than complexes with high internal (relative) energy content that would favor breakup through anisotropic coupling.

Our previous analysis of the PES features also indicates that the vibrational coupling appears to be rather localized in space, in the sense that T-shaped approaches show little coupling while collinear complexes exhibit the largest couplings between dimer vibrational levels and trimer relative motion. In this sense, we therefore expect similar results for VP processes as found here for RP processes. The actual calculations, however, require a more refined computation of the full PES and are now in progress in our laboratory.

ACKNOWLEDGMENTS

We are grateful to Dr. S. Serna-Molinera for his help in the initial fitting of the potential functions. The International Intensive Action Progamme between Italy and Spain is gratefully acknowledged for supporting exchange visits between the collaborating groups. The financial funding of the computing time by the Italian National Research Council (CNR) is also acknowledged.

[1] A. W. Castleman, Jr. and R. G. Keesee, Chem. Rev. **86**, 589 (1986).
[2] K. Stephan and T. D. Märk, Chem. Phys. Lett. **90**, 51 (1982).
[3] R. G. Keesee and A. W. Castleman, Jr., J. Phys. Chem. Ref. Data **15** 1011 (1986).
[4] S. Morgan and R. G. Keesee, and A. W. Castleman Jr., J. Am. Chem. Soc. **111**, 3841 (1989).
[5] U. Buck and H. Meyer, J. Chem. Phys. **84**, 4854 (1986).
[6] H. V. Böhmer and S. D. Peyerimhoff, Z. Phys D **3**, 195 (1986).
[7] Z. Y. Chen, C. R. Alberoni, M. Hasegawa, R. Kuhn, and A. W. Castleman, Jr., J. Chem. Phys. **91**, 4019 (1989).
[8] K. Stephan, T. D. Märk, E. Märk, A. Stamatovic, N. Djuric, and A. W. Castleman, Jr., Beitr. Plasmaphys. **23**, 369 (1983).
[9] K. Stephan, A. Stamatovic, A. W. Castleman, Jr., J. M. Furrell and T. D. Märk, Abstracts of Contributed Papers, XIII ICPEAC, edited by J. Eichler, W. Fritsch, I. V. Hertel, N. Stolterfoht, and U. Wille, Berlin, 1983 (unpublished), p. 291.
[10] E. E. Ferguson, C. R. Alberoni, R. Kuhn, Z. Y. Chen., R. G. Keesee, and A. W. Castleman, Jr., J. Chem. Phys. **88**, 6335 (1988).
[11] C. R. Alberoni, A. W. Castleman, Jr., E. E. Ferguson, Chem. Phys. Lett. **157**, 159 (1989).
[12] G. Delgado-Barrio, S. Miret-Artés, P. Villarreal, and F. A. Gianturco, Z. Phys. D **27**, 357 (1993).
[13] H. V. Böhmer and S. D. Peyerimhoff, Z. Phys. D **11**, 239 (1989).
[14] U. Buck and H. Meyer, Phys. Rev. Lett. **52**, 109 (1984).
[15] U. Buck and H. Meyer, Surf. Sci. **156**, 275 (1985).
[16] For example, see, R. J. Buenker, S. D Peyerimhoff, and W. Butscher, Mol. Phys. **35**, 771 (1978).
[17] H.-U. Böhmer, Dissertationarbeit, Bonn Universität, 1986.
[18] F. A. Gianturco, A. Palma, P. Villarreal, G. Delgado-Barrio, and O. Roncero, J. Chem. Phys. **87**, 1054 (1987).
[19] F. A. Gianturco, G. Delgado-Barrio, O. Roncero, and P. Villarreal, Int. J. Quantum Chem. **S21**, 389 (1987).
[20] F. A. Gianturco, G. Delgado-Barrio, O. Roncero, and P. Villarreal, Int. Rev. Phys. Chem. **7**, 1 (1988).
[21] F. A. Gianturco, G. Delgado-Barrio, O. Roncero, and P. Villarreal, Mol. Phys. **71**, 1405 (1990).
[22] D. Secrest, J. Chem. Phys. **62**, 710 (1975).
[23] L. W. Hunter, J. Chem. Phys. **62**, 2855 (1975).
[24] C. F. Curtiss, J. O. Hirschfelder, and F. T. Adler, J. Chem. Phys. **18**, 1638 (1950).
[25] R. T Pack, J. Chem. Phys. **60**, 633 (1974).